

# The *curved* Mimetic Finite Difference method: allowing grids with curved faces

Silvano Pitassi<sup>a,\*</sup>, Igor Petretti<sup>a</sup>, Francesco Trevisan<sup>a</sup>, Ruben Specogna<sup>a</sup>

<sup>a</sup>*University of Udine, Polytechnic Department of Engineering and Architecture, EMCLab, via delle scienze 206, 33100 Udine, Italy*

---

## Abstract

We present a new mimetic finite difference method able to deal with curved faces. Notably, it yields a symmetric discrete problem which uses only one degree of freedom for each curved face. The principle at the core of our construction is to abandon the standard definition of local consistency of mimetic finite difference methods. Instead, we exploit the novel and global concept of  $P_0$ -consistency. Numerical examples confirm the consistency and the convergence of the method for real-case problems with curved boundary geometries.

*Keywords:* mimetic discretizations, curved faces, dual grid

---

## 1. Introduction

The *Mimetic Finite Difference* (MFD) method [1] is a sound numerical technique that has been applied to solve many classes of physical problems. One of its advantages is the possibility of discretizing the computational domain with unstructured *polyhedral grids* having elements with planar faces. For these kind of elements, it yields a discrete convergent scheme which produces a *symmetric* matrix and uses one *degree of freedom* (DoF) for each face. Yet, many applications require grids whose elements have *curved* (i.e. non-planar) faces; for instance, the modeling of geometries like cylinders or spheres. We emphasize

---

\*Corresponding author: Tel.: +039-0432-558037;

*Email addresses:* [pitassi.silvano@spes.uniud.it](mailto:pitassi.silvano@spes.uniud.it) (Silvano Pitassi), [petretti.igor@spes.uniud.it](mailto:petretti.igor@spes.uniud.it) (Igor Petretti), [francesco.trevisan@uniud.it](mailto:francesco.trevisan@uniud.it) (Francesco Trevisan), [ruben.specogna@uniud.it](mailto:ruben.specogna@uniud.it) (Ruben Specogna)

that even if the computational domain is a polyhedron, curved faces may appear in the interior of the domain just because a hexahedral mesh has been obtained with an unstructured meshing algorithm. However, the standard MFD method does not converge on such grids with curved faces [2].

To deal with such convergence problems, different techniques have been proposed in literature. We can group them in two basic approaches.

A first approach is to replace curved faces by triangles (or more generally planar polygons) to obtain a polyhedral grid so that we can apply the standard MFD method [2]. Using this approach we obtain a symmetric discrete problem but the price to pay is the additional number of DoFs, which will be proportional to the number of polygons partitioning each curved face.

As a second approach, we can interpolate with standard least squares methods face DoFs inside each element to produce a constant vector field. Then, the mass matrix is obtained by projecting the constant vector field onto edges of a *dual* (or *secondary*) grid  $\tilde{K}$  [3]. A dual grid  $\tilde{K}$  is constructed by duality starting from a given discretization grid  $K$ , hence, called a *primal* grid. Here, duality is expressed as a bijective correspondence between geometric elements of the pair of grids  $(K, \tilde{K})$  such that to each  $d$ -dimensional geometric element in  $K$  corresponds a unique dual  $(3 - d)$ -dimensional geometric element in  $\tilde{K}$ . However, by using this dual grid approach on curved meshes, the resulting discrete problem is non-symmetric which significantly reduces the number of available efficient solution methods. Basically, the discretization methods in [4, 5] reduce to the above approach although a dual grid is not explicitly introduced.

The aim of this paper is to introduce the *curved* MFD method, an extension of the MFD method which yields a discrete problem which is symmetric and uses only one DoF for each curved face. Our work answers to an open question raised in [6, 2] on “whether the use of additional degrees of freedom is the only way to preserve symmetry in the discrete problem”. To the best of our knowledge, [6] is the only mimetic low-order numerical method that can handle curved grids. In [6], a symmetric discrete problem which uses three DoFs for

each curved face (more precisely, *strongly* curved faces<sup>1</sup>) is presented. There are other effective approaches for the accurate treatment of curved domains but restricted to the Finite Element framework [7], to 2-dimensional grids [8] or to high-order methods [9]. We note that the lowest order version of the approach in [9] employs more than one DoF for each curved face and thus is not equivalent to the curved MFD method proposed in this paper.

The principle at the core of our construction is to abandon the definition of *consistency* used in the standard MFD method. Consistency is a local property of *mimetic inner products* and *reconstruction operators* that encodes an exactness property for constant vector fields [1]. Fundamentally, consistency of the standard MFD method is equivalent to consistency enforced on the *barycentric dual grid*. In fact, in [10] it was shown that reconstruction operators of the standard MFD method are equivalent to reconstruction operators defined by geometric elements of the barycentric dual grid, as the ones used in the Discrete Geometric Approach (DGA) [11]. Reconstruction operators defined by the barycentric dual grid satisfy two key properties [10]:

- (P1) They provide a left inverse for local projection operators restricted to the vector subspace of constant vector fields, which is the *accuracy* or *unisolvence* property for constant vector fields [12].
- (P2) Their geometric entries form closed paths or surfaces supported on different elements.

The equivalence between these two kinds of reconstruction operators shows that focusing on local consistency leads essentially to one of the two approaches outlined above, which, however, have been explored in literature and do not achieve a discrete problem which is both symmetric and uses one DoF for each curved face. Indeed, property (P1) is not valid on grid elements having curved

---

<sup>1</sup>[6] distinguishes between *moderately* and *strongly* curved faces; the distinction between the two types of curved faces is based, as the names suggest, on a measure of curvature of the face and is used as a definition for theoretical analysis of convergence.

faces.

Instead of focusing on local consistency, we employ the novel concept of  $P_0$ -consistency introduced in [10]. Contrary to consistency of the standard MFD method,  $P_0$ -consistency is a global property since it involves reconstruction operators defined on more than one grid element. The idea underlying the definition of  $P_0$ -consistency is to abstract the properties **(P1)** and **(P2)** of the barycentric dual grid and reverse our line of reasoning: any grid whose geometric elements satisfy properties **(P1)** and **(P2)** leads to consistent reconstruction operators, precisely,  $P_0$ -consistent reconstruction operators.

A geometric characterization of  $P_0$ -consistent reconstruction operators can be given as the affine solution space of a linear system of equations. In Section 3 we give a purely combinatorial characterization of grids for which there exists a solution of this linear system, or equivalently, there exist  $P_0$ -consistent reconstruction operators. This combinatorial condition depends solely on the number of geometric element of the curved grid and requires that the number of curved faces is greater than three times the number of elements in  $K$ . If we assume that the curved grid  $K$  is made of elements having  $k$  curved faces each, the above combinatorial condition is satisfied for  $k \geq 6$ . Once  $P_0$ -consistent reconstruction operators are available, local mass matrices are constructed as in the standard MFD method. Hence, all the solid foundation of the standard MFD can be applied also to our novel curved MFD method.

In Section 4 we tested the curved MFD method on curved grids having highly curved faces and also curved boundaries. For all the considered examples consistency and convergence are achieved.

We note that the ability of expressing the MFD method using the geometric language is very important for improving its basic building blocks. Thus we emphasize the importance of seeing the geometry hidden behind the standard MFD method.

## 2. Notation

Let  $\Omega$  be a bounded polyhedral domain of  $\mathbb{R}^3$  with Lipschitz boundary. We assume that  $\Omega$  is simply connected. A  $k$ -cell is a  $k$ -dimensional manifold in  $\mathbb{R}^3$  that is homeomorphic to the closed  $k$ -dimensional ball. We equip each  $k$ -cell in  $K$  with an inner orientation [13]. A *cell complex*  $K$  on  $\Omega$  is a finite collection of  $k$ -cells for  $k = 0, 1, 2$  or  $3$  such that the following conditions hold [14]:

- Distinct  $k$ -cells in  $K$  have disjoint interiors.
- The boundary of any  $k$ -cell in  $K$  is a union of  $l$ -cells in  $K$  with  $l < k$ .
- The union of all cells in  $K$  is  $\Omega$ .
- The intersection of  $k$ -cell and an  $l$ -cell in  $K$  with  $l \leq k$  (if not empty) is a union of cells in  $K$ .

Crucially,  $k$ -cells as defined above can be *curved*. However, the standard MFD and DGA methods [11] require  $k$ -cells to be *planar* (or *flat*). A  $k$ -cell in  $K$  is planar if it is contained in a  $k$ -dimensional hyperplane of  $\mathbb{R}^3$ . For our purposes, 2-cells in  $K$  can be either flat or curved; consequently, also 1-cells in  $K$  can be either flat, like in a standard polyhedral cell, or curved. For each 3-cell of  $K$  we assume the same geometric regularity assumptions described in [6].

We denote the cell complex  $K$  as  $K = (N, E, F, C)$ , where  $N$  the set of 0-cells (*nodes*),  $E$  the set of 1-cells (*edges*),  $F$  the set of 2-cells (*faces*) and  $C$  the set of 3-cells (*elements*) in  $K$ .

We denote by  $|\cdot|$  either the cardinality of a set or the measure of a geometric element in  $K$ . For instance,  $|F|$  is the number of faces in  $K$ ,  $|f|$  is the area of face  $f \in F$  and  $|c|$  is the volume of element  $c \in C$ .

Let  $X$  be any set among  $N, E, F$  or  $C$ , so that elements of  $X$  are  $k$ -cells with  $0 \leq k \leq 3$ . Give a  $l$ -cell  $y$  in  $K$ , we denote by  $X(y)$  the subset defined by

$$X(y) := \{x \in X \mid x \subset \partial y\}, \quad (1)$$

if  $k < l$ , otherwise,

$$X(y) := \{x \in X \mid y \subset \partial x\}. \quad (2)$$

As an instance,  $F(c) = \{f \in F \mid f \subset \partial c\}$  collects the faces of  $c$  and  $C(e) = \{c \in C \mid e \subset \partial c\}$  is the cluster of elements containing edge  $e$ .

Let us consider a Cartesian system of coordinates with specified origin and denote by  $\mathbf{x} = (x_1, x_2, x_3)^T$  the coordinates of its generic point. To each node  $n \in N$  corresponds the point  $\mathbf{n} \in \mathbb{R}^3$ . A face  $f \in F$  is either a curved or a flat 2-cell. The *face vector*  $\mathbf{f}$  is

$$\mathbf{f} := \int_f \mathbf{n}_f dS, \quad (3)$$

where  $\mathbf{n}_f$  denotes the unit vector of  $\mathbb{R}^3$  orthogonal to  $f$  (at each point) and oriented according to the right-hand rule with respect to its boundary  $\partial f$ . Note that the integral in (3) is the same for every 2-cell spanning the polygonal boundary of  $f$ , as a consequence of the Divergence Theorem.

We now introduce the basic building blocks of the standard MFD method. We give only specialized definitions that are adapted to our purposes. A detailed presentation of the MFD framework can be found in [1, 12].

We denote by  $\mathcal{N}, \mathcal{E}, \mathcal{F}$  and  $\mathcal{C}$  the vector spaces of DoFs corresponding to nodes, edges, faces and elements, respectively. There are also vector spaces  $\tilde{\mathcal{N}}, \tilde{\mathcal{E}}, \tilde{\mathcal{F}}$  and  $\tilde{\mathcal{C}}$  collecting DoFs corresponding to *dual nodes*, *dual edges*, *dual faces* and *dual elements* [10, 13].

We will now focus on the vector space of face DoFs  $\mathcal{F}$ . Similar definitions hold for other vector spaces of DoFs [10].

The matrix  $\mathbb{P}_c^{\mathcal{F}}$  associated with the restriction of the *local projection operator* to the vector subspace of constant vector fields on an element  $c$  is

$$\mathbb{P}_c^{\mathcal{F}} := \begin{pmatrix} \vdots \\ \mathbf{f}^T \\ \vdots \end{pmatrix}, \quad (4)$$

where each row is a face vector  $\mathbf{f}$  of faces  $f \in F(c)$ .

We denote by  $\mathbb{R}_c^{\mathcal{F}}$  the matrix associated with the *average of local reconstruction operators* on an element  $c$  as defined in [10]. The so-called accuracy

property **(P1)** requires that  $\mathbb{R}_c^{\mathcal{F}}$  is a left inverse of  $\mathbb{P}_c^{\mathcal{F}}$  for every  $c \in C$ . An additional property that reconstruction operators have to satisfy is  $P_0$ -consistency and it will be formally defined in Section 3.

Starting from local reconstruction operators  $\{\mathbb{R}_c^{\mathcal{F}}\}_{c \in C}$  there is a standard reasoning to construct the *face mass matrix*  $\mathbb{M}^{\mathcal{F}}$ . First, local mass matrices  $\mathbb{M}_c^{\mathcal{F}}$  are constructed for every  $c \in C$ . Then, mass matrix  $\mathbb{M}^{\mathcal{F}}$  is obtained by using a standard Finite Element assembly process.

Let us consider for each element  $c$  a symmetric and positive-definite matrix  $\mathbb{K}_c$  of order 3, representing an homogeneous material property in  $c$ . The local mass matrix  $\mathbb{M}_c^{\mathcal{F}}$  on a element  $c$  is defined starting from reconstruction operators as

$$\mathbb{M}_c^{\mathcal{F}} := |c|(\mathbb{R}_c^{\mathcal{F}})^T \mathbb{K}_c \mathbb{R}_c^{\mathcal{F}} + \mathbb{S}_c, \quad (5)$$

where  $\mathbb{S}_c$  is a *stabilization matrix* as defined in [1, 15]. Different choices are possible for  $\mathbb{S}_c$  depending on the specific physical problem under investigation [16].

For every  $c \in C$ , let  $\mathbb{O}_c^{\mathcal{F}}$  be the restriction matrix which maps face DoFs in  $\mathcal{F}$  to face DoFs restricted to  $c$ .  $\mathbb{O}_c^{\mathcal{F}}$  is a matrix of size  $|F(c)| \times |F|$  and every row has exactly one entry equal to 1 corresponding to a face of  $c$  and zero everywhere else.

We define the global mass matrix in terms of local mass matrices as follows

$$\mathbb{M}^{\mathcal{F}} = \sum_{c \in C} (\mathbb{O}_c^{\mathcal{F}})^T \mathbb{M}_c^{\mathcal{F}} \mathbb{O}_c^{\mathcal{F}}. \quad (6)$$

Discrete counterparts of differential operators are represented by incidence matrices as follows [1, 10, 13]. The *discrete gradient operator* is the matrix  $\mathbb{G}$  of size  $|E| \times |N|$  of incidence numbers between nodes and edges. The *discrete curl operator* is the matrix  $\mathbb{C}$  of size  $|F| \times |E|$  of incidence numbers between edges and faces. The *discrete divergence operator* is the matrix  $\mathbb{D}$  of size  $|C| \times |F|$  of incidence numbers between faces and elements.

Finally, we can define *derived discrete differential operators* through duality by using the mimetic inner product given by mass matrix  $\mathbb{M}^{\mathcal{F}}$  and the definitions of discrete differential operators as presented in [1, 12].

### 3. Curved MFD method

The novel curved MFD method is as follows. The definition of DoFs and discrete differential operators is the same of the standard MFD method. Instead, a new class of reconstruction operators is employed. Accordingly, discrete inner products and derived differential operators are defined starting from this class of reconstruction operators as described in Section 2.

We choose reconstruction operators among the class of the  $P_0$ -consistent reconstruction operators defined as follows; see also [17].

**Definition 3.1** ( $P_0$ -consistent face reconstruction operators). A collection of face reconstruction operators  $\{\mathbb{R}_c^{\mathcal{F}}\}_{c \in C}$  is said to be  $P_0$ -consistent if the following two conditions hold:

$$\begin{cases} \mathbb{R}_c^{\mathcal{F}} \mathbb{P}_c^{\mathcal{F}} = \mathbb{I}_3, \forall c \in C \\ \text{row}_e \mathbb{C}^T \left( \sum_{c \in C} (\mathbb{O}_c^{\mathcal{F}})^T |c| (\mathbb{R}_c^{\mathcal{F}})^T \right) = 0, \forall e \in E, e \not\subset \partial\Omega, \end{cases} \quad (7)$$

where  $\mathbb{I}_3$  denotes the identity matrix of order 3 and  $\mathbb{O}_c^{\mathcal{F}}$  is the restriction matrix defined in Section 2.

The definition of  $P_0$ -consistent reconstruction operators boils down to two requirements. First, each local reconstruction operator  $\mathbb{R}_c^{\mathcal{F}}$  is a left inverse of the local projection operator  $\mathbb{P}_c^{\mathcal{F}}$ , which is the accuracy property for element-wise constant vector fields (**P1**). Second, for each internal edge, row vectors of  $|c| \mathbb{R}_c^{\mathcal{F}}$  for  $c \in C(e)$  can be put one after the other to form a geometric closed path, namely, their vector sum is the zero vector (**P2**).

*Remark 1.* Note that the definition of  $P_0$ -consistency involves only the local projection matrices, as in (4), that collect local face vectors, as defined in (3). Hence, all the geometric information of curved faces is encoded into their face vectors so that  $P_0$ -consistency is well-defined on grids having curved faces.

Now we show that  $P_0$ -consistent reconstruction operators on every element are defined up to an arbitrary point in  $\mathbb{R}^3$ . This point can be used to optimize reconstruction operators and we explore this possibility in Section 4.

For every  $c \in C$ , let  $\mathbf{D}_c = (\dots, \mathbb{D}_{c,f}, \dots)^T$  be the vector of size  $|F(c)| \times 1$  collecting coefficients of row vector  $\text{row}_c \mathbb{D}$  corresponding to faces  $f \in F(c)$ . Given arbitrary nodes  $\{\mathbf{b}_c\}_{c \in C}$  in  $\mathbb{R}^3$  we have that

$$\mathbb{R}_{\mathbf{b}_c}^{\mathcal{F}} := \mathbb{R}_c^{\mathcal{F}} - \mathbf{b}_c \mathbf{D}_c^T, \forall c \in C, \quad (8)$$

is a well-defined family  $\{\mathbb{R}_{\mathbf{b}_c}^{\mathcal{F}}\}_{c \in C}$  of  $P_0$ -consistent reconstruction operators. This follows from the fact  $\mathbf{D}_c^T \mathbb{P}_c^{\mathcal{F}} = \mathbf{0}$ , which is true since by its very definition rows of  $\mathbb{P}_c^{\mathcal{F}}$  are exactly face vectors corresponding to faces  $f \in F(c)$ .

The two requirements (7) in Definition 3.1 can be encoded into a linear system of equations by introducing suitable matrices  $\mathbb{P}^{\mathcal{F}}$ ,  $\mathbb{R}^{\mathcal{F}}$  and  $\mathbb{I}$  defined as follows.

- Matrix  $\mathbb{P}^{\mathcal{F}}$  of size  $3|C| \times |F|$ .  $\mathbb{P}^{\mathcal{F}}$  is a block matrix defined as

$$\mathbb{P}^{\mathcal{F}} = \begin{pmatrix} \vdots \\ (\mathbb{P}_c^{\mathcal{F}})^T \mathbb{O}_c^{\mathcal{F}} \\ \vdots \end{pmatrix}. \quad (9)$$

See Fig. 1.

- Matrix  $\mathbb{R}^{\mathcal{F}}$  of size  $|F| \times 3$ .  $\mathbb{R}^{\mathcal{F}}$  is defined as

$$\mathbb{R}^{\mathcal{F}} = \begin{pmatrix} \vdots \\ \mathbf{b}_f^T \\ \vdots \end{pmatrix}, \quad (10)$$

where each vector  $\mathbf{b}_f$  corresponds to a face  $f \in F$ . If  $f$  is the common face between two elements  $c, c'$ , then we identify the columns of  $\mathbb{R}_c^{\mathcal{F}}$  and  $\mathbb{R}_{c'}^{\mathcal{F}}$  corresponding to face  $f$  with the same vector  $\mathbf{b}_f$ ; see Remark 2.

- Matrix  $\mathbb{I}$  of size  $3|C| \times 3$ .  $\mathbb{I}$  is a block matrix defined as

$$\mathbb{I} = \begin{pmatrix} \vdots \\ |c| \mathbb{I}_3 \\ \vdots \end{pmatrix}. \quad (11)$$

$$\begin{array}{c}
c'' \\
c \\
c'
\end{array}
\begin{pmatrix}
0 & -\mathbf{f}_j & 0 \\
\vdots & 0 & \mathbf{f}_k \\
\mathbf{f}_i & \vdots & \vdots \\
\cdots & \vdots & \cdots \\
-\mathbf{f}_i & \mathbf{f}_j & \cdots \\
\vdots & \vdots & \vdots \\
0 & 0 & 0
\end{pmatrix}$$

Figure 1: Structure of matrix  $\mathbb{P}^{\mathcal{F}}$ . Face vector of each internal face appears on two different rows with opposite sign, where the two rows correspond to the unique two elements sharing the internal face; instead, each boundary face appears only in one block corresponding to the unique element containing it. For instance, the internal face  $f_i$  is shared between elements  $c, c'$  and its face vector  $\mathbf{f}_i$  appears with opposite sign on different rows corresponding to elements  $c, c'$ ; the boundary face  $f_k$  is contained in the unique element  $c''$  and its face vector  $\mathbf{f}_k$  appears only in the rows corresponding to element  $c''$ .

We write the following linear system of equations

$$\mathbb{P}^{\mathcal{F}} \mathbb{R}^{\mathcal{F}} = \mathbb{I}, \tag{12}$$

which is equivalent to (7). Note that information on volumes of elements is encoded into matrix  $\mathbb{I}$ .

*Remark 2* (Dual grid structure associated with  $P_0$ -consistent reconstruction operators). Corresponding to  $P_0$ -consistent reconstruction operators solution of (12) there is a “generalized” dual grid structure as follows. We think each vector  $\mathbf{b}_f$  in (10) as a “generalized barycenter” of face  $f$  (hence, the notation  $\mathbf{b}_f$ ). We think each node  $\mathbf{b}_c$  as a “generalized barycenter” of element  $c$ . Next, we think each pair  $(\mathbf{b}_f, \mathbf{b}_c)$ , where  $f$  is a face of element  $c$ , as a “generalized dual edge” with suitable orientation given by the pair order and depending on the orientation of face  $f$ . See Section 4 for instances of such dual grid structures constructed for the considered test cases.

Let now study the existence of a solution of linear system (12). The matrices  $\mathbb{P}^{\mathcal{F}}, \mathbb{R}^{\mathcal{F}}$  and  $\mathbb{I}$  depend on the geometry of the input mesh  $K$ . Hence, conditions that guarantee existence of a solution restrict the class of input meshes. In order

to guarantee the existence of a solution of linear system (12) a necessary and sufficient condition is that  $\text{rank } \mathbb{P}^{\mathcal{F}} = 3|C|$ . Hence, a necessary condition is that  $|F| \geq 3|C|$ .

The next result shows that the condition  $|F| \geq 3|C|$  is also sufficient. It is the crucial result of the paper since it allows to extend the standard MFD method to curved faces.

It can be advisable to use Fig. 1 as an illustration of the structure of matrix  $\mathbb{P}^{\mathcal{F}}$  for the following proof.

**Theorem 1** (Existence of  $P_0$ -consistent reconstruction operators). *Let  $K = (V, E, F, C)$  be a curved grid such that*

$$|F| \geq 3|C|. \quad (13)$$

*Then, there exists a solution of linear system (12).*

*Proof.* Assume that, for the sake of contradiction,  $\text{rank } \mathbb{P}^{\mathcal{F}} < 3|C|$ . Hence, by definition of the block matrix  $\mathbb{P}^{\mathcal{F}}$  in (9), there exists an element  $c$  whose block  $(\mathbb{P}_c^{\mathcal{F}})^T \mathbb{O}_c^{\mathcal{F}}$  is linear combinations of other blocks  $(\mathbb{P}_{c'}^{\mathcal{F}})^T \mathbb{O}_{c'}^{\mathcal{F}}$  of  $\mathbb{P}^{\mathcal{F}}$  with  $c' \in C \setminus \{c\}$  as follows

$$(\mathbb{P}_c^{\mathcal{F}})^T \mathbb{O}_c^{\mathcal{F}} + \sum_{c' \in C \setminus \{c\}} p_{c'} (\mathbb{P}_{c'}^{\mathcal{F}})^T \mathbb{O}_{c'}^{\mathcal{F}} = \mathbf{0}, \quad (14)$$

for some real coefficients  $p_{c'}$ . Let  $S$  be the set of elements in  $C$  whose coefficient  $p_c$  is different from zero in (14), namely,  $S = \{c \in C \mid p_c \neq 0\}$ .  $S$  is not empty since  $c \in S$ . Moreover,  $S = C$ . Indeed, if that is not the case, then  $C \setminus S \neq \emptyset$ . Since  $K$  is connected, there exists  $c^* \in C \setminus S$  such that  $c^* \cap c'$  for some  $c' \in S$ . It follows that  $p_{c^*} \neq 0$  and thus  $c^* \in C$  as well. Now, since  $S = C$ , there exists a boundary face  $f'$  contained in some  $c' \neq c$  such that  $p_{c'} \neq 0$ . Since  $f'$  is a boundary face,  $c'$  is the unique element in  $C$  containing it. Hence, the column of  $(\mathbb{P}_c^{\mathcal{F}})^T \mathbb{O}_c^{\mathcal{F}}$  corresponding to the boundary face  $f'$  should be different from the zero vector since the expression (14) includes the block  $p_{c'} (\mathbb{P}_{c'}^{\mathcal{F}})^T \mathbb{O}_{c'}^{\mathcal{F}}$ . This gives the desired contradiction since  $c \neq c'$ .  $\square$

We now discuss the implications of the condition (13) on the geometry of  $K$ . Let us assume that each element  $c$  has the same number  $k$  of faces. Consider the set  $T$  of all pairs  $(c, f)$  where  $f$  is a face of  $c$ . Since every element has  $k$  faces,  $|T| = k|C|$ . But since each internal face is shared by exactly two elements and each boundary face is incident to exactly one element we have  $|T| = 2|F_i| + |F_b|$ , where sets  $F_i$  and  $F_b$  partition  $F$  into internal and boundary faces, respectively. By combining these equations and plugging into (13) we get the condition

$$(k - 6)|F_i| \geq (3 - k)|F_b|. \quad (15)$$

Summarizing the above reasoning, the following corollary follows immediately. It gives a special characterization of the class of grids  $K$  admitting  $P_0$ -consistent reconstruction operators.

**Corollary 1.** *Let  $K = (V, E, F, C)$  be a curved grid such that the boundary of every element  $c \in C$  decomposes into  $k$  faces. Then, there exists a solution of (12) if and only if  $k \geq 6$ .*

Corollary 1 implies that, given a curved grid such that the boundary of every element decomposes into  $k \geq 6$  faces, we can write a discrete problem which is symmetric and uses only one DoF for each curved face.

To practically deal with the cases  $k = 4$  or  $k = 5$ , we propose the following construction. We select a face  $f$  of each element  $c$  to form a sequence of pairs  $T = (\dots, (f, c), \dots)$ . Then, if  $k = 4$ , we partition each face appearing in a pair of the sequence  $T$  into three polygons, and we group them to form three linearly independent face vectors. Similarly, if  $k = 5$ , we partition each face appearing in a pair of the sequence  $T$  into two polygons, and we group them to form two linearly independent face vectors. At the end of the procedure, in both cases we get a curved grid where each element satisfies the condition  $k \geq 6$  so that we can apply Corollary 1. Note that a sequence  $T$  as above can be constructed efficiently in linear time and space using standard spanning tree constructions (e.g. see [17] for a detailed description of such a construction). The price to pay is the additional number of DoFs which shifts from  $|F|$  to  $|F| + 2|C|$  for  $k = 4$  and  $|F| + |C|$  for  $k = 5$ .

#### 4. Numerical results

In this section we present numerical experiments to test the consistency and performance of the curved MFD method. We consider a stationary conduction problem as a prototype example of an elliptic boundary value problem. The stationary conduction problem in a region  $\Omega$  (chosen as in Section 2) is

$$\nabla \times \mathbf{E} = \mathbf{0}, \quad (16a)$$

$$\nabla \cdot \mathbf{J} = 0, \quad (16b)$$

$$\mathbf{J} = \sigma \mathbf{E}, \quad (16c)$$

where  $\sigma$  is the material parameter electric conductivity,  $\mathbf{E}$  is the electrostatic field and  $\mathbf{J}$  is the current density vector. In all the considered test problems the conductivity is assumed to be  $\sigma = 1$  S/m.

We attach DoFs of  $\mathbf{E}$  and  $\mathbf{J}$  to dual edges  $\mathbf{E}^{\tilde{\mathcal{E}}}$  and to faces  $\mathbf{I}^{\mathcal{F}}$ , respectively [10, 18].  $\mathbf{E}^{\tilde{\mathcal{E}}}$  is expressed using the scalar potential  $U^{\tilde{\mathcal{N}}}$  on dual nodes as

$$\mathbf{E}^{\tilde{\mathcal{E}}} = -\mathbb{D}^T U^{\tilde{\mathcal{N}}} + \mathbf{E}_s^{\tilde{\mathcal{E}}}, \quad (17)$$

where  $\mathbf{E}_s^{\tilde{\mathcal{E}}}$  is used to enforce Dirichlet boundary conditions. We assume that electromotive forces  $\{U_i^{\tilde{\mathcal{N}}}\}_{i=1}^{N_e}$  corresponding to the electrodes  $\{\partial\Omega_i^c\}_{i=1}^{N_e}$  placed on  $\partial\Omega$  are assigned with respect to a reference electrode  $\partial\Omega_0^c$ . On the remaining part of the boundary,  $\partial\Omega \setminus \cup_{i=1}^{N_e} \partial\Omega_i^c$ , a homogeneous Neumann boundary condition is enforced. By using expression (17), discrete Faraday law  $\mathbb{C}^T \mathbf{E}^{\tilde{\mathcal{E}}} = \mathbf{0}$  holds implicitly, since  $\mathbb{C}^T \mathbb{D}^T = (\mathbb{D}\mathbb{C})^T = \mathbf{0}$  holds and  $\mathbf{E}_s^{\tilde{\mathcal{E}}}$  is such that  $\mathbb{C}^T \mathbf{E}_s^{\tilde{\mathcal{E}}} = \mathbf{0}$ .

Next, the current continuity law

$$\mathbb{D}\mathbf{I}^{\mathcal{F}} = \mathbf{0} \quad (18)$$

has to be enforced by the linear system of equations.

The face mass matrix  $\mathbb{M}^{\mathcal{F}}$  is constructed as follows. First,  $P_0$ -consistent face reconstruction operators are obtained as a solution of (12). Next, for each element  $c \in C$  we compute the average node  $\mathbf{b}_c := \frac{1}{|F(c)|} \sum_{f \in F(c)} \mathbf{b}_f$ . We use nodes  $\{\mathbf{b}_c\}_{c \in C}$  to define the new family  $\{\mathbb{R}_{\mathbf{b}_c}^{\mathcal{F}}\}_{c \in C}$  of  $P_0$ -consistent reconstruction operators as in (8). The rationale behind the definition of the nodes  $\{\mathbf{b}_c\}_{c \in C}$  stems

from the geometric interpretation of  $P_0$ -consistent reconstruction operators outlined in Remark 2; in [17] it is shown how the choice of such nodes is related to optimal properties of local reconstructed vector fields, like for instance, the reconstructed constant vector field is optimal as measured by a  $L^2$  norm. Finally, local mass matrices and global mass matrices are constructed from  $\{\mathbb{R}_{\mathbf{b}_c}^{\mathcal{F}}\}_{c \in C}$  using (5) and (6).

Similarly to *mixed Finite Elements* [19], we write a system with both  $\mathbf{I}^{\mathcal{F}}$  and  $U^{\tilde{\mathcal{N}}}$  as unknowns

$$\mathbb{M}^{\mathcal{F}} \mathbf{I}^{\mathcal{F}} - \mathbb{D}^T U^{\tilde{\mathcal{N}}} = \mathbf{E}_s^{\tilde{\mathcal{E}}}, \quad (19)$$

$$\mathbb{D} \mathbf{I}^{\mathcal{F}} = \mathbf{0}. \quad (20)$$

This saddle-point problem may be recasted as a symmetric and positive-definite system using mixed-hybrid Finite Elements [19].

#### 4.1. Patch test

We test the consistency of the curved mimetic method by solving a Poisson problem whose solution is uniform in  $\Omega$ . Since we consider a stationary current conduction problem, a simple way to produce a uniform vector fields is to consider a resistor with known symmetry.

We have considered a cubic domain  $\Omega$  and a curved grid subdivision on it as follows. Starting from a polyhedral grid made of hexahedral elements we have randomly perturbed internal nodes positions. In this way, each element has curved faces (and straight edges) since nodes of at least one face of every element are not all lying on a plane in  $\mathbb{R}^3$ . The boundary conditions have been set to generate a uniform current density of amplitude 1 A and pointing down the vertical axis.

Figure 2 shows the resulting reconstructed vector field together with the dual grid structure associated with  $P_0$ -consistent reconstruction operators. On the left picture we see that the uniform current density is reconstructed exactly in the whole curved grid  $K$ . We note that the standard MFD method and the approach proposed in [6] produce symmetric discrete problems that use more

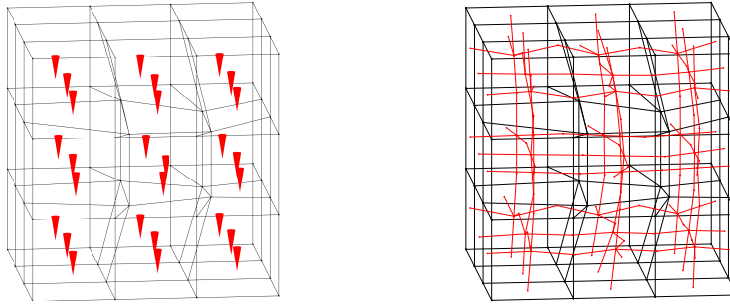


Figure 2: A curved grid partitioning the cube resistor where all internal faces of each element are curved. On the left, uniform current density reconstructed inside each curved element; it coincides with the analytical value. On the right, in red, dual grid structure associated with  $P_0$ -consistent face reconstruction operators solution of (12).

than one DoF for each curved face. Instead, our formulation employs just one DoF for each curved face.

If a standard barycentric dual grid is used to define local reconstruction operators, like in the DGA method, or, equivalently, like in the standard MFD method, then we use one DoF for each curved face. However, we do not achieve consistency in that the reconstructed field is not uniform. To quantitatively measure the consistency error we have considered the relative error on the dissipated power of the resistor. For the considered curved grid we get a 1% relative error.

It is interesting to remark that our method treats all curved faces in the same way, namely, does not distinguish between different types of curved faces. In [6], curved faces are partitioned in moderately and strongly curved faces depending on a user-dependent parameter quantifying the curvature of a curved face.

#### 4.2. Square resistor

Next, we consider a square resistor where a voltage of  $u = 1$  V is enforced between the electrodes placed in the two lateral surfaces of a solid squared torus.

As done in Section 4.1, we have considered a curved grid partitioning  $\Omega$  obtained by randomly perturbing internal nodes positions starting from an initial hexahedral grid. Figure 3 shows the resulting reconstructed vector field to

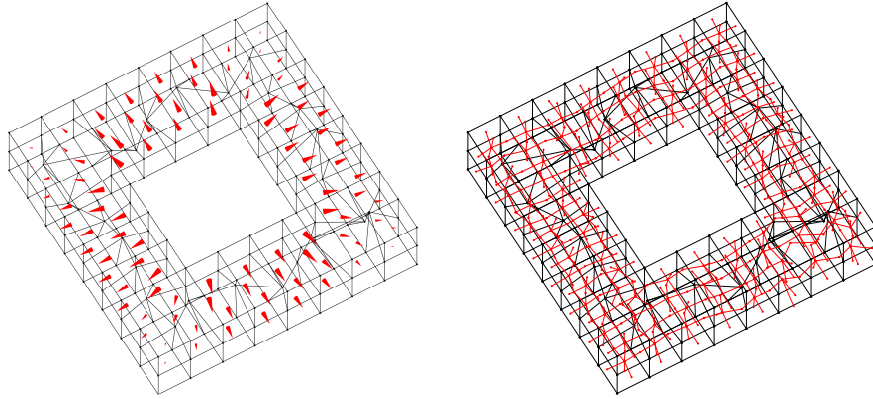


Figure 3: A curved grid partitioning the square resistor where all internal faces of each element are curved. On the left, current density reconstructed inside each curved element. On the right, in red, dual grid structure associated with  $P_0$ -consistent face reconstruction operators solution of (12).

gether with the dual grid structure associated with  $P_0$ -consistent reconstruction operators.

To compare the accuracy of the curved MFD method, we have computed its numerical approximation of the dissipated power of the square resistor and we have compared it with the same value computed with the standard MFD method by considering the relative error. The comparison is made by varying the number of curved faces that are approximated by piecewise linear surfaces. A curved face is approximated by a piecewise linear surface made of two triangles (since we perturbed an initial hexahedral grid) by connecting two of its vertices. As the number of curved faces approximated in this way increases, we gradually include more DoFs and we get a discrete problem of increasing size and increasing accuracy. Local reconstruction operators are defined by using face barycenters like in the standard MFD method. By treating all faces as curved we get a 3% relative error. Instead, by approximating all curved faces with piecewise linear surfaces we get basically the same value of dissipated power. Yet, the number of DoFs has doubled.

### 4.3. Spherical resistor

Finally, we test the performance of the curved MFD method with a computational domain having curved boundary. The aim of this test is to compare the performance of the curved MFD method on a domain with curved boundary, in comparison with the standard MFD method on polyhedral elements obtained by approximating the curved boundary with planar polygons. Moreover, we test the correctness of boundary conditions on curved boundary faces.

We have considered one eighth of a spherical resistor  $\Omega$  as in Fig. 4. The boundary  $\partial\Omega$  decomposes into an interior surface electrode  $\partial\Omega_0^c$  with radius 1 (the sphere is centered in the origin of the fixed spherical coordinate system) and into an external surface electrode  $\partial\Omega_1^c$  with radius 2. A voltage of  $u = 1$  V is enforced between the reference electrode  $\partial\Omega_0^c$  and  $\partial\Omega_1^c$ .

The domain is partitioned into a curved grid (whose skeleton is shown in Fig. 4) and into a polyhedral grid having the same nodes but curved faces are approximated by piecewise linear surfaces as described in Section 4.2. In this case, each element of the curved grid has curved faces but also curved edges.

Figure 5 shows the reconstructed vector field on curved elements together with the dual grid structure associated with  $P_0$ -consistent reconstruction operators.

In Fig. 6 we plot the convergence of the dissipated power versus grids of increasing size of the curved and standard MFD method. Interestingly, for coarse grids the curved MFD method gives a better accuracy in the computed dissipated power given that is not affected by the geometric error made in the approximation of the curved electrode surface  $\partial\Omega_1^c$  by polygons. For increasing grid sizes, this error tends to zero and the two curves coincide yielding the same convergence behavior.

## 5. Conclusions

A new MFD method able to deal with curved faces has been introduced. Notably, it yields a discrete problem which is symmetric and uses one DoFs for

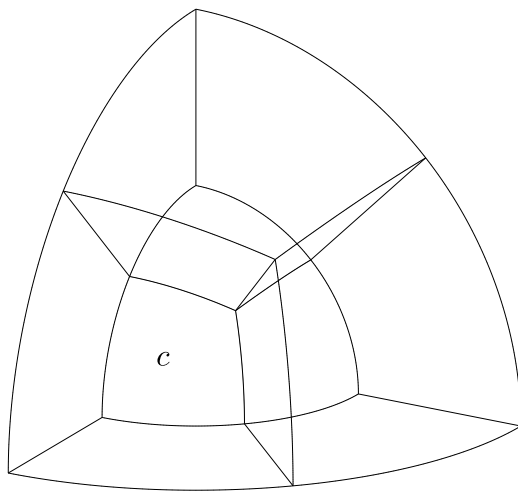


Figure 4: Skeleton of a coarse curved grid partitioning one eighth of a spherical resistor. On the bottom left a curved element  $c$ ; each curved element has both curved faces and edges.

each curved face. This has been achieved by employing the new geometrical and topological concept of  $P_0$ -consistent reconstruction operators. As a result, the concept of dual grid has been generalized to curved faces. The consistency of the new scheme has been tested numerically, demonstrating that the exact solution of the patch test is recovered for domain discretization grids having curved faces. The convergence results show that the curved MFD method is able to get the same accuracy of the standard MFD method where curved faces are partitioned into planar polygons but without introducing additional DoFs.

A range of work is slated for future investigation, focusing on further improvements to the properties of  $P_0$ -consistent reconstruction operators. It is also expected that the methods described here can be generalized to high-order methods. However, it is expected that geometric interpretation of the high-order method to be more challenging.

## References

- [1] K. Lipnikov, G. Manzini, M. J. Shashkov, Mimetic finite difference method, *J. Comput. Phys.* 257 (2014) 1163–1227.

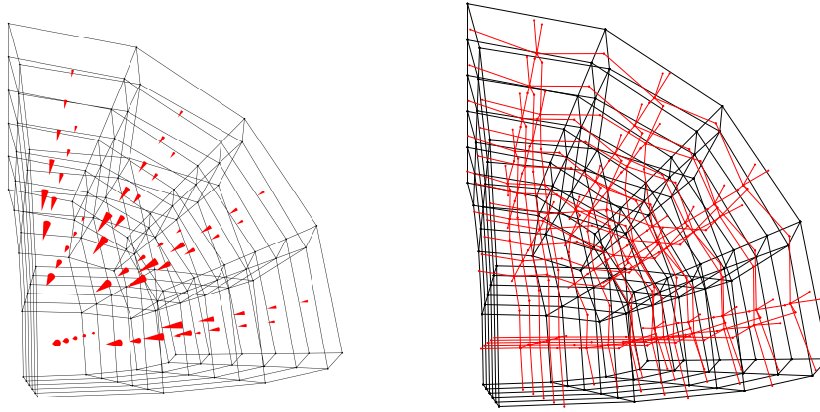


Figure 5: A curved grid partitioning one eighth of a spherical resistor where all internal faces of each element are curved just like in Fig. 4 (the grid nodes are connected by straight edges only for visualization purposes). On the left, current density reconstructed inside each curved element. On the right, in red, dual grid structure associated with  $P_0$ -consistent face reconstruction operators solution of (12). Note that dual nodes lie on the curved boundary surface  $\partial\Omega_1^c$  in order to enforce Dirichlet boundary conditions on the scalar potential.

- [2] K. Lipnikov, M. J. Shashkov, D. Svyatskiy, The mimetic finite difference discretization of diffusion problem on unstructured polyhedral meshes, *J. Comput. Phys.* 211 (2006) 473–491.
- [3] S. Pitassi, F. Trevisan, R. Specogna, Explicit geometric construction of sparse inverse mass matrices for arbitrary tetrahedral grids, *Computer Methods in Applied Mechanics and Engineering* 377 (2021) 113699.
- [4] I. D. Mishev, Nonconforming finite volume methods, *Computational Geosciences* 6 (2002) 253–268.
- [5] I. Aavatsmark, An introduction to multipoint flux approximations for quadrilateral grids, *Computational Geosciences* 6 (2002) 405–432.
- [6] F. Brezzi, K. Lipnikov, M. J. Shashkov, Convergence of mimetic finite difference method for diffusion problems on polyhedral meshes with curved faces, *Mathematical Models and Methods in Applied Sciences* 16 (2006) 275–297.

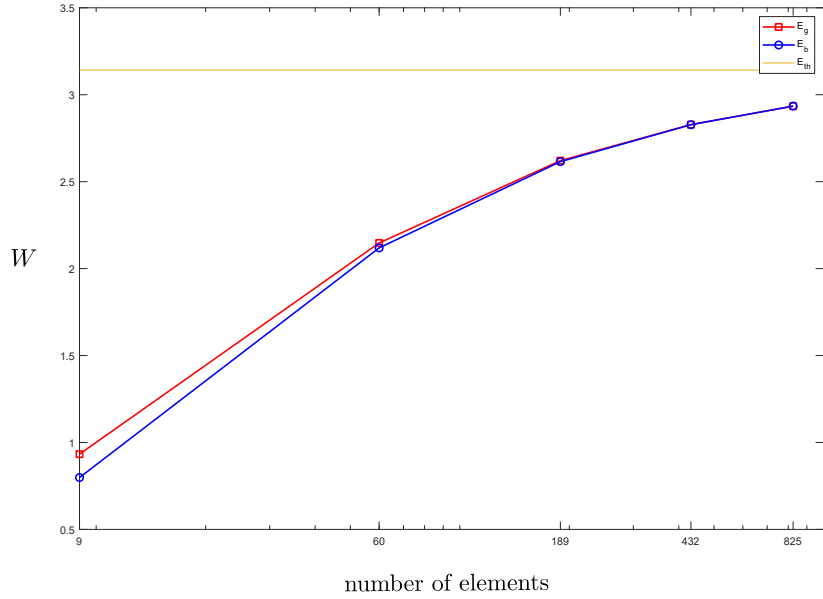


Figure 6: Convergence of the numerical approximation of the dissipated power for grids of increasing size.  $E_{th}$  is the reference value equal to  $\pi W$  for the considered one eighth of the spherical resistor domain  $\Omega$ .  $E_g$  and  $E_b$  represent dissipated power of the curved and standard MFD method, respectively.

- [7] R. Sevilla, S. Fernández-Méndez, A. Huerta, Comparison of high-order curved finite elements, *International Journal for Numerical Methods in Engineering* 87 (2011) 719–734.
- [8] L. B. da Veiga, A. Russo, G. Vacca, The virtual element method with curved edges, *ESAIM: Mathematical Modelling and Numerical Analysis* (2019).
- [9] L. Botti, D. A. D. Pietro, Assessment of hybrid high-order methods on curved meshes and comparison with discontinuous galerkin methods, *J. Comput. Phys.* 370 (2018) 58–84.
- [10] S. Pitassi, R. Ghiloni, F. Trevisan, R. Specogna, The role of the dual grid

- in low-order compatible numerical schemes on general meshes, *J. Comput. Phys.* 436 (2021) 110285.
- [11] L. Codecasa, R. Specogna, F. Trevisan, A new set of basis functions for the discrete geometric approach, *J. Comput. Phys.* 229 (2010) 7401–7410.
- [12] L. B. da Veiga, K. Lipnikov, G. Manzini, *The mimetic finite difference method for elliptic problems*, volume 11, Springer, 2014.
- [13] E. Tonti, *The mathematical structure of classical and relativistic physics: A general classification diagram*, 2013.
- [14] S. H. Christiansen, A construction of spaces of compatible differential forms on cellular complexes, *Mathematical Models and Methods in Applied Sciences* 18 (2008) 739–757.
- [15] J. Bonelle, D. A. Di Pietro, A. Ern, Low-order reconstruction operators on polyhedral meshes: application to compatible discrete operator schemes, *Computer Aided Geometric Design* 35 (2015) 27–41.
- [16] J. Bonelle, D. A. D. Pietro, A. Ern, Low-order reconstruction operators on polyhedral meshes: application to compatible discrete operator schemes, *Comput. Aided Geom. Des.* 35-36 (2015) 27–41.
- [17] S. Pitassi, R. Ghiloni, R. Specogna, Inverting the discrete curl operator: a novel graph algorithm to find a vector potential of a given vector field, *ArXiv abs/2111.04431* (2021).
- [18] A. Bossavit, How weak is the “weak solution” in finite element methods?, *IEEE Trans. Magn.* 34 (1998) 2429–2432.
- [19] F. Brezzi, M. Fortin, *Mixed and hybrid finite element methods*, in: Springer Series in Computational Mathematics, 1991.